
Article:
Imam, S.A. orcid.org/0000-0003-1198-7448, Hughes, A.C. orcid.org/0000-0001-7507-2496, Carré, M.J. orcid.org/0000-0003-3622-990X et al. (4 more authors) (2023) Finite element model to simulate impact on a soft tissue simulant. Sports Engineering, 26 (1). 16. ISSN 1369-7072

https://doi.org/10.1007/s12283-023-00407-7

Sports Engineering (2023) 26:16
https://doi.org/10.1007/s12283-023-00407-7

TECHNICAL NOTE

Finite element model to simulate impact on a soft tissue simulant

Syed Adil Imam[1,2] · Angus C. Hughes[3] · Matthew J. Carré[3] · Heather Driscoll[4] · Keith Winwood[2] · Prabhuraj Venkatraman[2] · Tom Allen[2]

Accepted: 13 February 2023

Abstract
A finite element model of an impact test on a soft tissue simulant, used as part of a shoulder surrogate, was developed in Ansys© LS-DYNA®. The surrogate consisted of a metal hemicylindrical core, with a diameter of 75 mm, covered with a 15 mm thick relaxed muscle simulant. The muscle simulant consisted of a 14 mm thick layer of silicone covered with 1 mm thick chamois leather to represent skin. The material properties of the silicone were obtained via quasi-static compression testing (curve fit with hyperelastic models) and compressive stress relaxation testing (curve fit with a Prony series). Outputs of the finite element models were compared against experimental data from impact tests on the shoulder surrogate at energies of 4.9, 9.8 and 14.7 J. The accuracy of the finite element models was assessed using four parameters: peak impact force, maximum deformation, impact duration and impulse. A 5-parameter Mooney-Rivlin material model combined with a 2-term Prony series was found to be suitable for modelling the soft tissue simulant of the shoulder surrogate. This model had under 10% overall mean deviation from the experimental values for the four assessment parameters across the three impact energies. Overall, the model provided a repeatable test method that can be adapted to help predict injuries to skin tissue and the performance/efficacy of personal protective equipment.

1 Introduction

World Rugby™ have a Body Padding Performance Specification [1] (WR-BPPS), to govern the body padding sometimes worn by rugby union players. WR-BPPS provides requirements for the design, material specifications and performance test methods for body padding. It also notes that body padding is only intended to protect against cuts and abrasions. As such, World Rugby™ does not intend for body padding to protect again severe injuries like dislocations and fractures. With technological and material advancements and developments in playing style, WR-BPPS must be reviewed to ensure it fulfils its intended purpose. The specification includes an impact acceleration attenuation test, with a flat-faced metal impactor dropping onto the padding when placed onto a cylindrical metal anvil (Ø 115 mm). This anvil is intended to mimic the shoulder shape.

The impact test setup, with the metal anvil, in WR-BPPS is well suited for test houses, where test equipment must be durable and highly repeatable, but it does not fully reflect gameplay interaction. Indeed, the test does not fully represent rugby tackles, or other collisions, especially those that cause cuts and abrasions. Using cadaveric or post-mortem human specimens are not ideal for assessing the effect of protective equipment design on performance in relation to cuts and abrasions [2–4]. The reasons they are not ideal include the natural biological and anthropometric variation between individuals, ethical considerations, differences between live and post-mortem tissue, degradation/damage from storage, and repeated testing. Using a more biofidelic anvil [3, 5, 6] could help improve our understanding of how rugby padding might perform during impact when worn by a player. Indeed, Hughes et al. [7] developed a relaxed muscle simulant (by mixing silicones) for assessing

This article is a part of a Topical Collection in Sports Engineering on The Engineering of Sport 14 Conference held at Purdue University USA, edited by Dr Hugo Espinosa, Steven Shade, Dr Kim Blair, Professor Jan-Anders Månsson.

✉ Syed Adil Imam
Adil.imam@canterbury.ac.uk

1 Canterbury Christ Church University, Canterbury CT1 1QU, UK

2 Manchester Metropolitan University, Manchester M1 5GD, UK

3 Department of Mechanical Engineering, University of Sheffield, Sheffield S1 3JD, UK

4 Advanced Manufacturing Research Centre (AMRC), Sheffield S60 5BL, UK

Published online: 02 March 2023

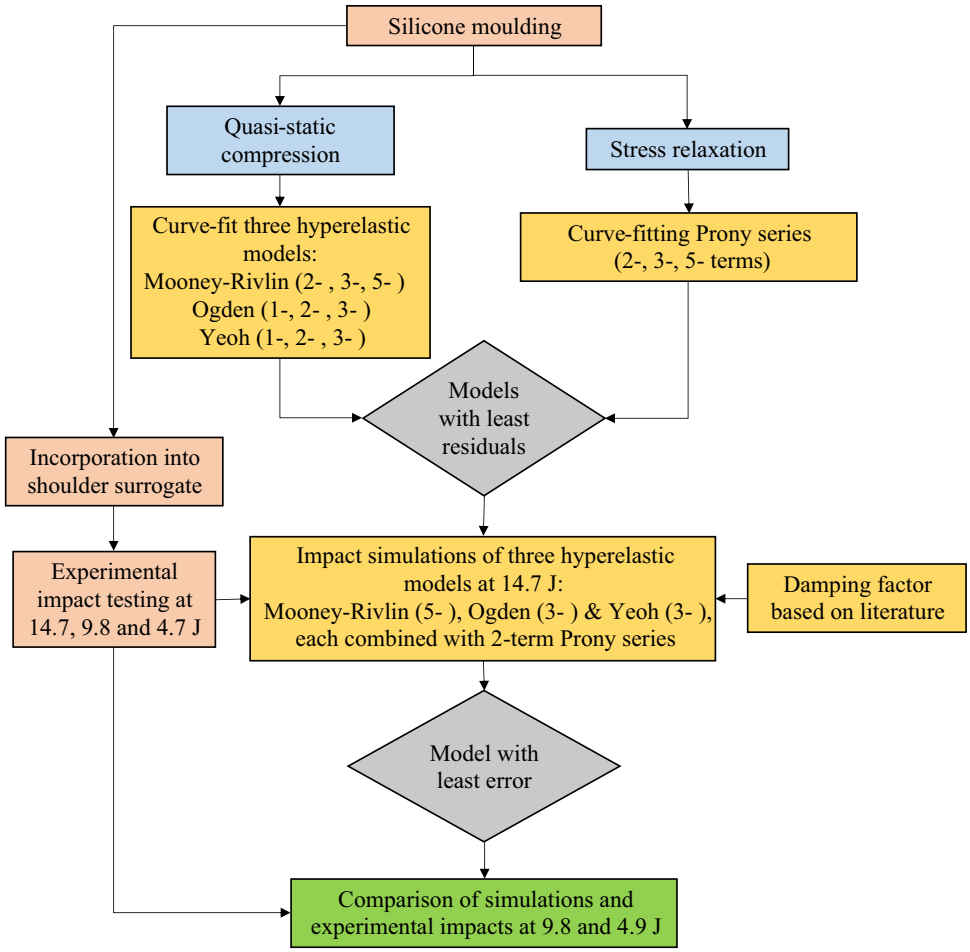

Fig. 1 Flowchart summarising the methodology used to model and validate the shoulder surrogate

the ability of rugby body padding to prevent injury. In recent work investigating raking injuries from studs, Hughes et al. [8] covered the muscle simulant with a layer of synthetic chamois leather to represent skin [9, 10]. Placing such a synthetic tissue or silicone over a metal anvil, whilst not completely mimicking the shoulder anatomy, would give a more biofidelic anvil than the metal cylinder currently used in the WR-BPPS.

Biofidelic anvils incorporating compliant materials are less durable than metal anvils, and they can degrade when impacted repeatedly [11, 12]. A finite element (FE) model that simulates an impact test with a biofidelic anvil would allow the effect of various parameters, such as anvil size and shape, and changes to padding design, to be investigated in an efficient and repeatable manner. The literature [12–18] suggests that hyperelastic material models, such as Ogden [2, 17, 19–21] and Mooney-Rivlin [3, 22, 23], are suitable for modelling the stress vs. strain response of human soft tissue and associated simulants under slow loading. Such hyperelastic models can also be combined with viscoelastic ones [2, 3, 24–26] to simulate the response of soft tissue simulants under fast loading. While various material models have been reviewed for simulating soft tissue simulants, it is unclear which option is best, particularly for predicting impact response.

The aim of this paper was to develop an FE model to simulate impact tests on an anvil that was more biofidelic than the current metal one in WR-BPPS. The anvil consisted of a metal hemicylindrical core covered with the silicone reported by Hughes et al. [7, 8] and a synthetic chamois leather to mimic skin [9, 10]. An initial stage in developing such an FE model was to identify a suitable material model for predicting the impact response of the silicone.

2 Methods

The methods section consists of two sub-sections: (i) material testing and modelling—where curve fitting experimental stress–strain data of the silicone to hyperelastic material models are explained and (ii) FE modelling and validation—where the FE modelling setup and comparison against an experimental impact test based on the one detailed in WR-BPPS are presented (Fig 1). Some of the methods described in the following sections were based on findings from pilot tests and simulations, and these instances are noted.

2.1 Material testing and modelling methods

2.1.1 Sample preparation and density measurement

Four cylindrical samples of the silicone formulation used to mimic relaxed muscle tissue [7] were moulded for quasi-static and stress relaxation compression testing. These samples had a diameter of 29 mm and a height of 12.5 mm, as reported previously [4] and as per ASTM D395 [27]. The samples were weighed using a balance (ABS 220-4N, KERN®, Germany. Accuracy ± 0.1 mg). The diameter and height of the samples were measured using a vernier calliper (Composite Digital Vernier Calliper, Silverline®. Accuracy: ± 0.01 mm) and the volume was calculated. Using the measured mass and volume, the density of the silicone was calculated.

2.1.2 Quasi-static compression

Compression testing was undertaken using a Hounsfield Universal testing machine with a 10 kN load cell (accuracy ± 50 N). One sample was compressed once at strain rates of 0.0067, 0.067 and 0.67 s^{-1} (5, 50 and 500 mm/min test speed) up to 50%, to assess the rate dependency of the silicone. The strain rate of 0.067 s^{-1} was reported previously [4] and 500 mm/min was the machine maximum. The other three samples were compression tested at the highest speed of 500 mm/min until 70% compression. Repeats were carried out at the highest strain rate as pilot work showed that using the lower strain rate stress vs. strain curve resulted in high errors in predicting the peak force during impact with the FE model. Each sample was compressed three times (total of nine curves), with at least a minute between tests. The first compression test on each sample was not analysed, to avoid stress softening effects, i.e. Mullin's effect [28] (leaving six curves in total). The median stress vs. strain curve across all three samples was selected (visually) for material modelling.

The compression platens were greased on their contact faces to limit friction with the sample and reduce any barrelling effect. An approach speed of 1 mm/min was applied until a preload of ~ 1 N to ensure the upper compression platen contacted the sample before testing. The force and displacement data were taken from the test machine to calculate engineering stress and strain from the measured sample dimensions. The synthetic chamois leather (IC200, Kent Car Care, Manchester, UK) was too thin (~ 1 mm) to compression test in isolation. Compression testing was, therefore, undertaken with a layer of chamois leather placed on top of a silicone sample to compare with the stress vs. strain curve of the silicone in isolation.

2.1.3 Stress relaxation testing

Three silicone samples were each compressed to 50% strain [3] at a strain rate of 6.7 s^{-1} (1000 mm/min, which was the machine maximum) using a hydraulic compression machine (Instron®, 10 kN load cell with accuracy: ± 100 N), and then held for 60 s. The force curve during the 60 s hold was converted to shear modulus (μ), using a Young's modulus (~ 1.1 MPa) calculated in the ramp time (from the gradient of a linear trend line) and an assumed Poisson's ratio of 0.48 (which for silicone ranges between 0.48 and 0.495 [29, 30] and is similar to the values reported for human skin [4, 31]) with:

$$\mu = \frac{E}{2(1+\upsilon)}. \quad (1)$$

The median shear stress vs. time curve was selected (visually) from the three samples and used for Prony series curve fitting in a viscoelastic material model (Fig. 1).

2.2 Experimental impact testing and simulation methodology

2.2.1 Experimental impact testing

Compliant anvils were fabricated by moulding the silicone formulation (14 mm thick and 150 mm long) [7] around a steel hemicylinder (Ø 75 mm) (Fig. 2). The silicone used for the anvil was from the same batch used to mould the material testing samples. Chamois leather was placed inside the mould before the silicone, causing it to join to the uppermost surface of the silicone (Fig. 2A, B). The inner surface of the silicone was bonded with adhesive spray to the steel hemicylinder creating a compliant anvil with the same external dimensions as the metal one specified in WR-BPPS (Fig. 2C, D). Three samples were moulded from the same batch of silicone, giving three compliant anvils. The consistency of the quasi-static compressive response of these three anvils is shown in Online Resource 1 Fig. S1. The base of the steel hemicylinder was fixed to a steel table via four load cells (208C05-Force Sensor, PCB Piezotronics) (Fig. 2E).

The compliant anvils were impacted at energies of 4.9, 9.8 and 14.7 J, by dropping a 5 kg mass (flat face, Ø 130 mm) from 0.1, 0.2 and 0.3 m, respectively (assuming no friction between the impactor and guide rails) (Fig. 2E). Each of the three compliant anvils was impacted three times at one of the three energies, with at least a minute between impacts (nine impacts in total). The load cells sampled at 20 kHz and were connected to an oscilloscope (PicoScope®, Version 6, Pico Technology) via one 3-Channel (480B21, PCB® Peizotronics) and one 1-Channel (480E09, PCB® Peizotronics) ICP® sensor signal conditioners (480B21,

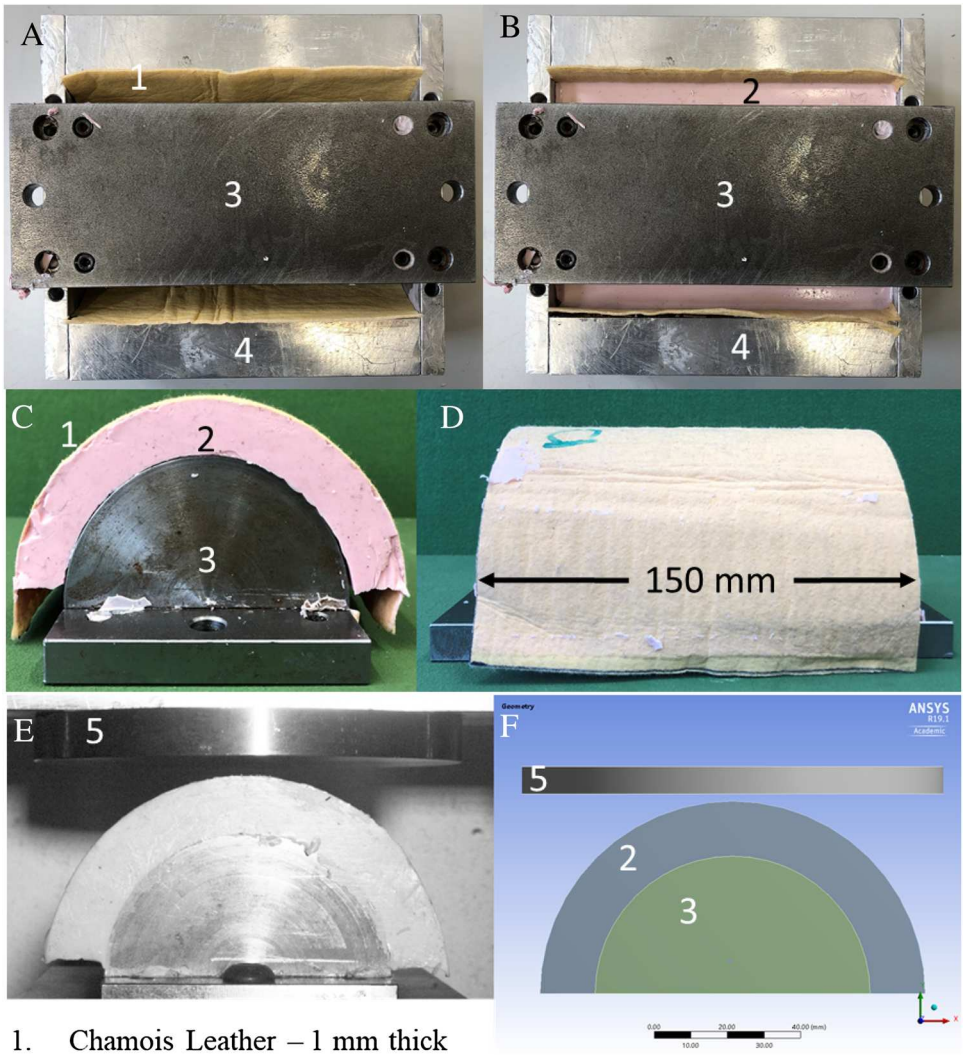

1. Chamois Leather – 1 mm thick
2. Relaxed muscle simulant – Silicone – 14 mm thick
3. Steel hemicylinder – Ø 75 mm
4. Mould used for curing silicone
5. Impactor - Ø 130 mm

Fig. 2 Making and modelling the compliant anvil. Moulding process—**A** just the chamois leather layer, **B** mould containing silicone. Compliant anvil—**C** end view, **D** side view, **E** high-speed camera image before impact. **F** End view of FE model

PCB®) to record impact force. The voltage readings from each load cell were converted to force using the calibration factor (range 0.2214–0.2399 mVN^{-1}) from the supplier and summed to give the total force at each 0.05 ms timestep. To measure impactor velocity and maximum deformation of the compliant layer of the anvil, each impact was filmed with a high-speed camera (Phantom Miro R111, Vision Research, USA) with a zoom lens (Nikon AF Nikkor 24–85 mm 1:2.8–4 D, Nikon Corporation, Japan) (example camera view in Fig. 2E). The camera was set to a resolution of 512 × 320 pixels, a sample rate of 10 kHz and an exposure rate of 99 µs. The camera and load cells were synchronized using the oscilloscope. Room temperature was checked hourly during testing, and stayed within 20 ± 2 °C, which is the ambient condition in WR-BPPS.

Peak impact force, impact duration, impulse, and maximum deformation (see definitions in Online Resource-1) for all nine experimental impacts were noted and tabulated for comparison to the FE model.

2.2.2 Modelling the impact test

The geometry of the anvil and impactor was modelled in SolidWorks© (Version 2018, Dassault Systems) and imported into Workbench (Version 19.1, Ansys©). The centre of the impactor was aligned to that of the anvil in the widthwise (x-axis) and lengthwise (z-axis) directions, and the impactor was placed 2 mm above (y-axis) the anvil.

The steel impactor and hemicylinder were assigned rigid material models, with the properties of steel (*MAT_RIGID,

$\rho = 7{,}850$ kg/m^3, $E = 200$ GPa and $\nu = 0.3$). The assigned density of the impactor was then artificially increased (to 64,829 kg/m^3), as the geometry of the entire drop carriage was not modelled, to give the required mass of 5 kg from the experiment. The default element type (hexahedral/ELFORM = 1) was applied to the impactor and hemicylinder, with a mesh size of 6 mm. The silicone layer was assigned a tetrahedral mesh (ELFORM = 10), to prevent negative volume errors [32], of element size 3 mm based on a mesh convergence study. These settings gave a total of 26,148 nodes and 108,980 elements with a mean quality of 0.85 ± 0.09 and a mean skewness of 0.215 ± 0.12 (mesh details and partwise breakdown in Online Resource-1 Table-S1).

Contact (*CONTACT_AUTOMATIC_SURFACE_TO_SURFACE) was defined between the silicone and impactor, and between the silicone and hemicylinder. The coefficients of friction between the soft tissue simulant and these metal parts (Chamois leather-impactor and silicone hemisphere) in the experimental setup were not measured and were therefore unknown. As such, estimated values for these coefficients of friction were used in the model. For simplicity, the static and dynamic coefficient of friction were both set to the same value, which was 0.3 (pilot simulations demonstrated low sensitivity- < 15 N (< 0.3%) in temporal force to changes in this value within the range of 0.2 and 0.6). The steel hemicylinder was fully constrained. The impactor was constrained to allow only vertical displacement and assigned an initial velocity (*INITIAL_VELOCITY_RIGID_BODY) equating to that of the theoretical value (ignoring friction) for the corresponding impact energy (Details in Online Resource-1 Table S2). Manual tracking of the drop mass in the video footage (Phantom CineViewer, Version 3.7, Ametek Vision Research, USA), for the first impact at each energy, indicated friction in the guide rails reduced the experimental impact velocity by no more than 0.1 ms^{-1} (~ 4%) from the theoretical value used in the model (Online Resource-1 Table S2). The time step safety factor was set to 0.4, reduced from the default value of 0.9 to prevent elements from passing through each other upon initial contact. Other contact settings were set as default.

The median stress vs. strain data from the quasi-static compression test on the silicone was imported into Ansys© Workbench v19.1 as uniaxial test data. Mooney-Rivlin (2-, 3- and 5-parameter), Ogden (1-, 2- and 3-parameter) and Yeoh (1-, 2- and 3-parameter) hyperelastic models were each fitted to the data using the curve-fit command. For each of these three hyperelastic models, the number of terms that gave the lower residual for the curve fit was chosen. The stress relaxation data was imported into Workbench using the viscoelastic shear data function. The Prony series relaxation curve-fit option was used with different numbers of terms (2–5), and the one with the lowest residual (2-term) for the curve fit was chosen.

Frequency-independent damping (input as a shear modulus) was added to reduce impact-induced vibrations of the silicone observed in pilot simulations. The damping also increased the stiffness of the silicone and hence increased peak impact forces (Online Resource-1 Fig. S2). When the shear modulus of the silicone (0.06 MPa) was calculated from Young's modulus measured during quasi-static compression testing (0.18 MPa at a strain rate of 0.67 s^{-1}) (Eq. 1), the peak impact forces during a pilot simulation at 14.7 J was lower (> 30%) than for the corresponding experiments. As such, the shear modulus used for damping was increased to bring the peak impact force from the model closer to that of the experiment. The maximum value found in the literature for Young's modulus of human skin tissue under dynamic loading was 140 MPa [33, 34]. Converting the maximum Young's Modulus of 140 MPa to shear modulus using 0.48 as the Poisson's ratio (Eq. 1), the value of 47 MPa was obtained and applied to the material model.

Simulations using the three hyperelastic material models (with least residuals, i.e., 5-parameter Mooney-Rivlin, 3-parameter Ogden and 3-parameter Yeoh), each combined with a 2-term Prony series, were run at 14.7 J impact energy (as per the WR-BPPS test method) to determine which one gave the closest agreement to the experimental impact data. The material model in closest agreement with the experimental data at 14.7 J (5-parameter Mooney-Rivlin hyperelastic material model combined with a 2-term Prony series) was then compared to the experiments at 4.9 and 9.8 J. The. d3plot output files from the simulations were postprocessed in LS-Prepost, where the temporal contact force between the silicone and impactor was obtained. Using the integration option, the area under the curve (impulse) was computed. Outputs from the FE model were only compared against the first experimental impact at each energy, to limit any effect of silicone degradation (as observed in pilot testing at 14.7 J with another sample).

3 Results

3.1 Material modelling results

The density of the silicone was calculated as $1{,}072 \pm 75$ kg/m^3 (mean ± S.D.). The gradient of the stress vs. strain curve, and hence the silicone stiffness, increased with the strain (non-linear) (Fig. 3A, B) and strain rate (rate dependent) (Fig. 3A). The stress vs. strain curve of the silicone with the chamois leather on top was similar to that of the silicone in isolation, with a slight change at ~ 65% strain, when the chamois leather tore (Fig. 3C). This tear at ~ 65%

compression resulted in a drop in the stress vs. strain curve, which affected the curve fitting during material modelling. As such, only the silicone compression data was used for material modelling. For stress relaxation testing, the shear modulus (peak value of ~ 0.6 MPa) decayed rapidly during the constant strain hold phase after the load application and then relaxed to a steady value of ~ 0.33 MPa after approximately a second. As such, the stress relaxation data was cropped to just five seconds after the loading period for curve fitting to the Prony series. The 5-parameter Mooney-Rivlin curve fit gave a lower residual (8) than the 3-parameter Ogden and 3-parameter Yeoh (22 and 24, respectively) when fitted to the quasistatic compression test data. For Prony series curve fitting, a 2-term fit followed the stress relaxation test data more closely than a 3- or 5-term. All hyperelastic and Prony series curve fit images and coefficients are in Online Resource 1, Figs. S3–6, and Tables S3–5.

3.2 Experimental and FE simulation results

Peak force, maximum deformation and impulse increased with impact energy, while impact duration decreased (Online Resource-1 Table-S6). Of the three hyperelastic material models (5-parameter Mooney-Rivlin, 3-parameter Ogden and 3-parameter Yeoh, each combined with a 2-term Prony series) assigned to the silicone at 14.7 J, the 5-parameter Mooney-Rivlin model was in closest agreement with the experimental data, with a mean difference of ~ 7% across the four assessment parameters. Visual comparisons of temporal forces at all three impact energies, and video footage from the experiment and animations from the simulations for impacts at 14.7 J, indicate reasonable agreement (Fig. 4) (Online Resource 2).

The Ogden model returned the same impact duration as the experiment, whereas the Yeoh model returned a 7% error. For both models, larger discrepancies in the other three parameters (> 25%) increased the overall difference and made them unsuitable for modelling the silicone (Online Resource-1 Table-S7). The 5-parameter Mooney-Rivlin with a 2-term Prony series model at 9.8 and 4.9 J resulted in mean differences of 10 and 9% across the four assessment parameters, respectively (Table 1).

4 Discussion

A 5-parameter Mooney-Rivlin hyperelastic material model combined with a 2-term Prony series was found to be the best predictor of the silicone, for impact energies of 14.7 J across four measuring parameters. The Mooney-Rivlin hyperelastic material model was expected to outperform the Ogden and Yeoh models under impact, as it provided a closer fit to the quasi-static stress vs. strain curve of the silicone (Online Resources 1 Figs. S2–4). This model showed under 10% discrepancy with the experimental values across

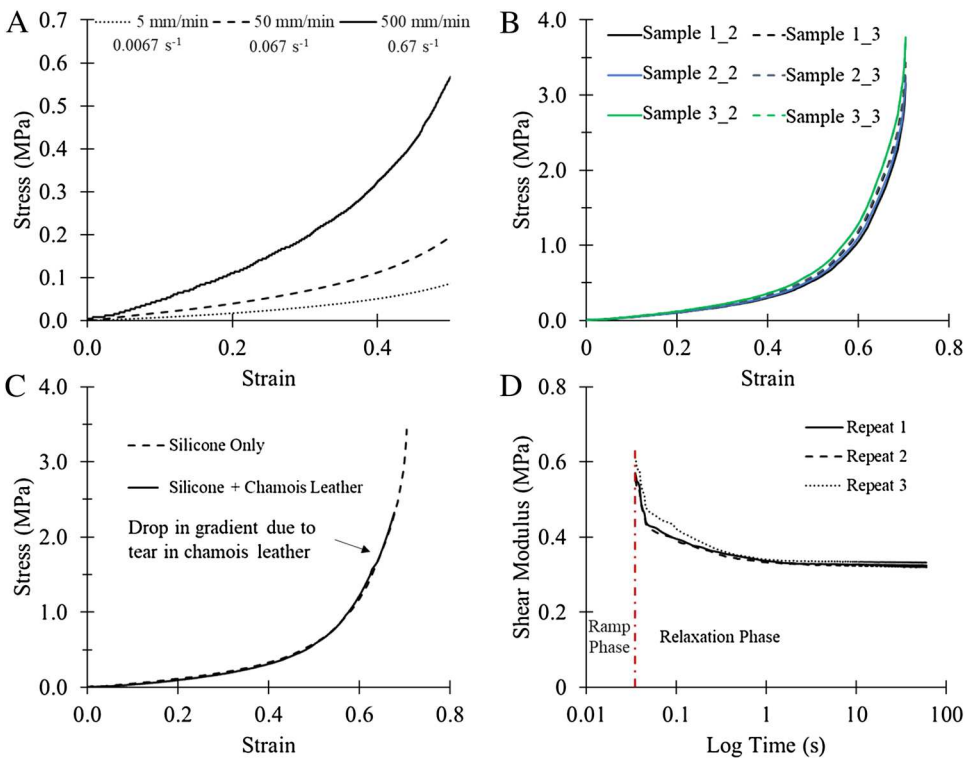

Fig. 3 Compressive stress vs. strain curve of the silicone samples **A** at strain rates up to 50% compression, **B** up to 70% compression at 500 mm/min (0.67 s^{-1}) (3 samples × 2 repeats each), **C** compared to the curve of a silicone sample with the chamois layer at 500 mm/min (0.67 s^{-1}). Only the median curve is plotted to show the drop in stress value. **D** Shear Modulus curve of the silicone under stress relaxation testing

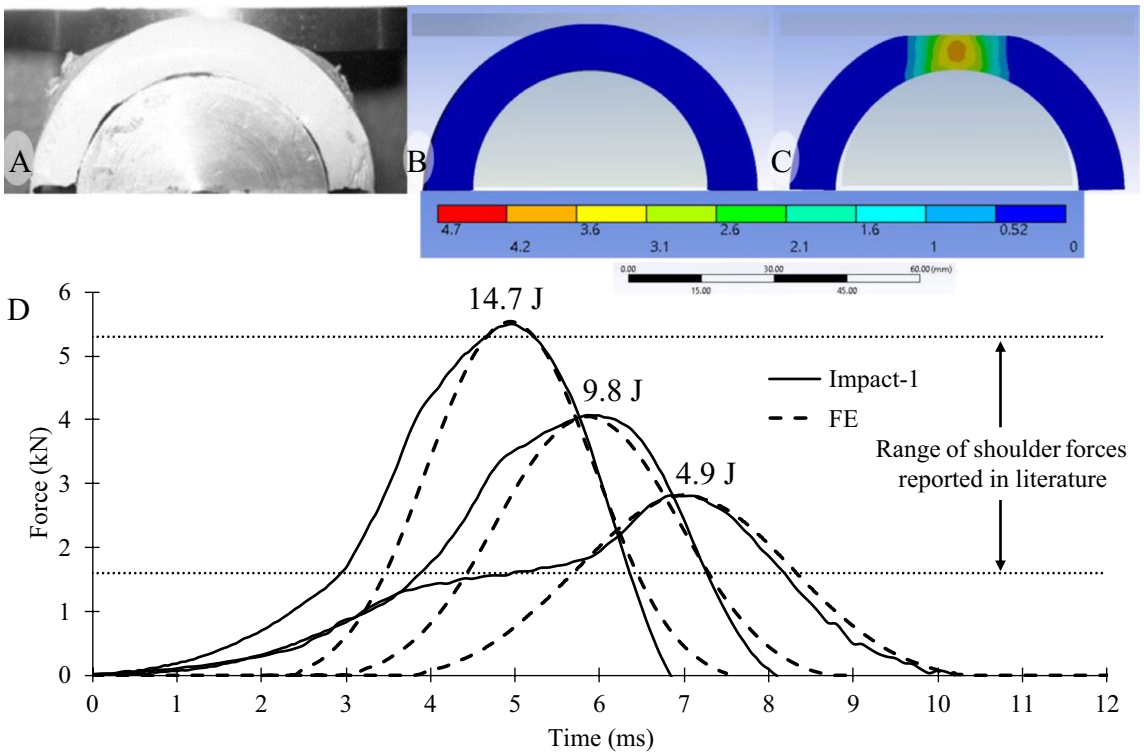

Fig. 4 Results of a 14.7 J impact; maximum compression between **A** experimental impact high-speed video front view with different orientations in FE simulation; **B** front view with no sectioning **C** front view with sectioning-slice of the central plane to enable visualisation of von-Mises stresses induced. **D** Comparison of experimental and FE simulation graphs showing temporal force data at 14.7, 9.8 and 4.9 J—FE force trace translated to align with experimental peak force. Dotted horizontal lines represent the range of peak shoulder forces shown in the literature for a tackle on a tackle bag or a scrum replication on a scrum machine [35–40]

Table 1 Comparison of 5-parameter Mooney-Rivlin 2-term Prony model against experimental impact data at 14.7, 9.8 and 4.9 J

Energy J	Model	Peak force N (Error %)	Deformation mm (Error %)	Impact duration ms (Error %)	Impulse Ns (Error %)	Mean error %
14.7	Experimental	5499	5.1	6.8	16	7
	FE model	5538 (+1)	4.7 (− 7)	6.3 (− 7)	13 (− 14)	
9.8	Experimental	4071	3.5	8.1	13	10
	FE model	4040 (− 1)	3.8 (+9)	6.8 (− 16)	11 (− 12)	
4.9	Experimental	2399	2.9	10.5	11	9
	FE model	2460 (+3)	3.1 (− 7)	9.0 (+11)	9 (− 18)	
				Overall error mean		8.6

all four measuring parameters for the three impact energies of 4.9, 9.8 and 14.7 J, with the best agreement for peak force (within 3%) and the worst for impulse (within 20%). The peak impact force observed during the 14.7 J test (5.5 kN) was similar (5.3 ± 1 kN) to peak force values reported at the shoulder for a tackle on a bag [35, 36] (Fig. 3). The peak forces observed for the 4.9 and 9.8 J tests (2.4–4.0 kN) fell within the lower range of peak shoulder forces (1.6 to 4.6 kN) reported elsewhere in the literature for a tackle on a bag or a scrum replication on a scrum machine [37–40] (Fig. 4). A comparison of temporal forces for the experimental impacts in this study to those of a scrum from reference [40] is presented in Online Resource-1 Fig. S8. Future work in this area would benefit from the knowledge of typical interaction forces between players during rugby specific scenarios, rather than when a player interacts with a tackle bag or a scrum machine.

When simulating an impact at 14.7 J, the inputs of the material model applied to the silicone had to be tuned to increase the peak force in line with the experimental value, by increasing frequency-independent damping. This requirement to tune the material model inputs to align the results to

experimental data means it may not be accurate for impact energies and scenarios that fall outside those tested here, and this could be determined in future work. Even with frequency-independent damping and a strain rate dependency (in terms of a Prony series fit to stress relaxation data) included in the material model, the simulations with the Ogden and Yeoh models unpredicted peak impact force by 27 and 35%, respectively. Characterising the silicone at a higher strain rate, which could include using impact test data [41–43] to obtain the stress vs. strain relationship, could remove, or lessen, the need for tuning the material model with frequency-independent damping. Quasi-static compression of the silicone at different strain rates was only conducted up to 50% compression (Fig. 3a), with compression up to 70% only at the highest strain rate of 500 mm/m (Fig. 3b). Future work could also benefit from characterising the silicone at lower strain rates up to higher levels of compression (e.g., 70%). For example, slow compression and slow impact simulations on silicone may benefit from lower strain rate material data.

The Poisson's ratio of silicone has been reported to be between 0.48 to 0.496 [29, 30] and simulations at 14.7 J using values of 0.48 and 0.49 showed minimal change in the shape of the force trace and the four measuring parameters (< 0.05%) (Online Resource- Fig. S7). Despite the model outputs being insensitive to changes in Poisson's ratio within the expected values for silicone, future work could measure the value for the specific blend used here, to see if it falls within this range. Static and dynamic frictional coefficients, between the soft tissue simulant and metal parts, were also estimated in the model (as 0.3). Future work should measure these frictional coefficients and apply them to the model.

Many of the material models in the literature that have been fitted to quasi-static data for soft tissue simulants and have not been implemented into FE models for simulating impact, as done in this study. Further work could focus on incorporating rugby padding into the FE model, and including damage modelling, as applied to simulate wooden baseball bat failure [44], to simulate soft tissue injuries. Such future work could determine whether a 10% deviation from the experiment, as reported here, is sufficient to assess the ability of various designs of padded clothing to reduce the risk of soft tissue injuries, or whether further improvement of the model is required. While the anvil used here is not an exact replica of the shoulder anatomy, the model could be developed to better mimic the shoulder or other anatomical regions, particularly those where soft tissue injuries can be sustained whilst playing rugby. The process of developing the model to better represent the human anatomy could benefit from data collected from testing cadavers.

5 Conclusion

An FE model of a compliant surrogate, consisting of silicone covering a steel hemicylinder, with the same diameter as the metal anvil defined in the World Rugby™ body padding performance specification has been compared against experimental impact test data. A 5-parameter Mooney-Rivlin material model combined with a 2-term Prony series was the best predictor of the impact performance of the silicone at three impact energies, up to 14.7 J. The model can be used to study impact force propagation through the silicone and could be developed to analyse protective equipment for sports and other scenarios where the shoulder anatomy is concerned. The validated model presented here could be further developed to test the efficacy of padding against soft tissue injuries, such as cuts and abrasions, by incorporating damage modelling.

Supplementary Information The online version contains supplementary material available at https://doi.org/10.1007/s12283-023-00407-7.

Acknowledgements We would like to thank World Rugby™ for funding this research. In addition, the technical team at Manchester: Stephen Moyle, Bob Bamford & Anthony Dickenson for fabricating and developing the drop rig and Michael Green for assistance during testing.

Data availability The datasets generated during and/or analysed during the current study are available from the corresponding author upon reasonable request.

Declarations

Conflict of interest The work was funded by World Rugby™ . One of the authors serves as an editor for *Sports Engineering*, and was blinded from the peer-review process.

References

1. World Rugby (2019) Body padding performance specifications. https://www.world.rugby/the-game/player-welfare/equipment/specifications/body-padding
2. Shergold OA, Fleck NA, Radford D (2006) The uniaxial stress versus strain response of pig skin and silicone rubber at low and high strain rates. Int J Impact Eng 32:1384–1402

3. Payne T, Mitchell S, Bibb R, Waters M (2015) The evaluation of new multi-material human soft tissue simulants for sports impact surrogates. J Mech Behav Biomed Mater 41:336–356
4. Annaidh AN, Destrade M, Ottenio M et al (2014) Strain rate effects on the failure characteristics of excised human skin. In: Proceedings of the 9th international conference on the mechanics of time dependent materials (MTL), Montréal, QC, Canada. pp 27–30
5. Payne T, Mitchell S, Halkon B, et al (2016) Development of a synthetic human thigh impact surrogate for sports personal protective equipment testing. Proc Inst Mech Eng Part P J Sport Eng Technol 230:5–16
6. Michio Clark J, Connor TA, Post A et al (2020) Could a compliant foam anvil characterize the biofidelic impact response of equestrian helmets? J Biomech Eng. https://doi.org/10.1115/1.4045403/1067324
7. Hughes A, Driscoll H, Carré M (2020) Development of silicone elastomer for use in the assessment of padded clothing in Rugby Union. In: Multidisciplinary digital publishing institute proceedings, p 77
8. Hughes AC, Dixon J, Driscoll HF et al (2022) Padded rugby clothing to prevent laceration and abrasion injuries from stud raking: a method of assessment. Sport Eng 25:3. https://doi.org/10.1007/s12283-022-00369-2
9. Ankersen J, Birkbeck AE, Thomson RD, Vanezis P (1999) Puncture resistance and tensile strength of skin simulants. Proc Inst Mech Eng Part H J Eng Med 213:493–501
10. Oudshoorn B, Driscoll H, Dunn M et al (2018) Development of a test method for assessing laceration injury risk of individual cleats during game-relevant loading conditions. Footwear Sci 10:1–10
11. Payne T, Mitchell S, Bibb R, Waters M (2014) Initial validation of a relaxed human soft tissue simulant for sports impact surrogates. Proc Eng 72:533–538
12. Payne T, Mitchell S, Bibb R, Waters M (2015) Development of novel synthetic muscle tissues for sports impact surrogates. J Mech Behav Biomed Mater 41:357–374
13. Marchesseau S, Heimann T, Chatelin S et al (2010) Fast porous visco-hyperelastic soft tissue model for surgery simulation: application to liver surgery. Prog Biophys Mol Biol 103:185–196
14. Larrabee WF Jr, Galt JA (1986) A finite element model of skin deformation. III. The finite element model. Laryngoscope 96:413–419
15. Lapeer RJ, Gasson PD, Karri V (2010) Simulating plastic surgery: from human skin tensile tests, through hyperelastic finite element models to real-time haptics. Prog Biophys Mol Biol 103:208–216
16. Hendriks FM, Brokken D, Van Eemeren J et al (2003) A numerical-experimental method to characterize the non-linear mechanical behaviour of human skin. Ski Res Technol 9:274–283
17. Evans SL (2009) On the implementation of a wrinkling, hyperelastic membrane model for skin and other materials. Comput Methods Biomech Biomed Eng 12:319–332
18. Benítez JM, Montáns FJ (2017) The mechanical behavior of skin: structures and models for the finite element analysis. Comput Struct 190:75–107
19. Evans SL, Holt CA (2009) Measuring the mechanical properties of human skin in vivo using digital image correlation and finite element modelling. J Strain Anal Eng Des 44:337–345
20. Mahmud J, Holt CA, Evans SL (2010) An innovative application of a small-scale motion analysis technique to quantify human skin deformation in vivo. J Biomech 43:1002–1006
21. Joodaki H, Panzer MB (2018) Skin mechanical properties and modeling: a review. Proc Inst Mech Eng Part H J Eng Med 232:323–343
22. Payne T, Mitchell S, Bibb R (2013) Design of human surrogates for the study of biomechanical injury: a review. Crit Rev Biomed Eng 41:51–89
23. Groves RB, Coulman SA, Birchall JC, Evans SL (2012) Quantifying the mechanical properties of human skin to optimise future microneedle device design. Comput Methods Biomech Biomed Engin 15:73–82
24. Silver FH, Freeman JW, DeVore D (2001) Viscoelastic properties of human skin and processed dermis. Ski Res Technol 7:18–23
25. Khatyr F, Imberdis C, Vescovo P et al (2004) Model of the viscoelastic behaviour of skin in vivo and study of anisotropy. Ski Res Technol 10:96–103
26. Delalleau A, Josse G, Lagarde J et al (2008) A nonlinear elastic behavior to identify the mechanical parameters of human skin in vivo. Ski Res Technol 14:152–164
27. ASTM-International (2018) ASTM D395-Standard Test Methods for Rubber Property. Compression Set
28. Mullin L, Tobin NR (1965) Stress softing in rubber vulcanizates I. Use of stain-amplification factor to describe the elastic behavior of filler-reinforced vulcanizated rubber. J Appl Polym Sci 9:2993
29. Larson K (2019) Can You Estimate Modulus From Durometer Hardness for Silicones? In: Dow White Pap. https://www.dow.com/content/dam/dcc/documents/en-us/tech-art/11/11-37/11-3716-01-durometer-hardness-for-silicones.pdf. Accessed 30 Sep 2022
30. O'Hara G (1983) Mechanical properties of silicone rubber in a closed volume. Tech Report, Army Armament Res Dev Cent
31. Delalleau A, Josse G, Lagarde J-M et al (2006) Characterization of the mechanical properties of skin by inverse analysis combined with the indentation test. J Biomech 39:1603–1610
32. LSTC (2018) LS-DYNA keyword user's manual-volume-II material models
33. Kalra A, Lowe A, Al-Jumaily AM (2016) Mechanical behaviour of skin: a review. J Mater Sci Eng 5:1000254
34. Jacquemoud C, Bruyere-Garnier K, Coret M (2007) Methodology to determine failure characteristics of planar soft tissues using a dynamic tensile test. J Biomech 40:468–475
35. Seminati E, Cazzola D, Preatoni E, Trewartha G (2016) Specific tackling situations affect the biomechanical demands experienced by rugby union players. https://doi.org/10.1080/14763141.2016.1194453
36. Seminati E, Cazzola D, Trewartha G et al (2017) Biomechanical loads in rugby union tackling are affected by tackle direction and impact shoulder. ISBS Proc Arch 35:81
37. Usman J, McIntosh AS, Fréchède B (2011) An investigation of shoulder forces in active shoulder tackles in rugby union football. J Sci Med Sport 14:547–552
38. Usman J, McIntosh AS, Quarrie K, Targett S (2015) Shoulder injuries in elite rugby union football matches: epidemiology and mechanisms. J Sci Med Sport 18:529–533
39. Weldon C, Archbold K, Tierney G, et al (2019) Forward and inverse dynamics reconstruction of a staged rugby tackle. In: Conference proceedings international research council on the biomechanics of injury, IRCOBI. pp 622–623
40. Lallemand B, Clanet C, Blanchard S et al (2020) Peak compression force physics in Rugby Union Scrum. Proc 49:151. https://doi.org/10.3390/PROCEEDINGS2020049151
41. Shepherd T, Winwood K, Venkatraman P et al (2020) Validation of a finite element modeling process for auxetic structures under impact. Phys Status Solidi 257:1900197. https://doi.org/10.1002/PSSB.201900197
42. Ankrah S, Mills NJ (2003) Performance of football shin guards for direct stud impacts. Sport Eng 6:207–219
43. Smith L, Burbank S (2013) Simulating sport ball impact through material characterization. Proc Eng 60:73–78
44. Fortin-Smith J, Sherwood J, Drane P, Kretschmann D (2018) Characterization of maple and ash material properties for the finite element modeling of wood baseball bats. Appl Sci 8:2256